

ARTICLE OPEN

New insights into natural variability and anthropogenic forcing of global/regional climate evolution

Tongwen Wu¹, Aixue Hu¹, Feng Gao^{1,2,3,4,5}, Jie Zhang¹ and Gerald A. Meehl²

Because of natural decadal climate variability—Atlantic multi-decadal variability (AMV) and Pacific decadal variability (PDV)—the increase of global mean surface air temperature (GMSAT) has not been monotonic although atmospheric greenhouse-gas (GHG) concentrations have been increasing continuously. It has always been a challenge regarding how to separate the effects of these two factors on GMSAT. Here, we find a physically based quasi-linear relationship between transient GMSAT and well-mixed GHG changes for both observations and model simulations. With AMV and PDV defined as the combination of variability over both the Atlantic and Pacific basins after the GHG-related trend is removed, we show that the observed GMSAT changes from 1880 to 2017 on multi-decadal or longer timescales receive contributions of about 70% from GHGs, while AMV and PDV together account for roughly 30%. Moreover, AMV contributes more to time-evolving GMSAT on multi-decadal and longer timescales, but PDV leads AMV on decadal timescales with comparable contributions to GMSAT trends.

npj Climate and Atmospheric Science (2019) 2:18; <https://doi.org/10.1038/s41612-019-0075-7>

INTRODUCTION

Although the influence of decadal climate variability on regional and global climate has been studied previously,¹ additional attention has been brought to bear on this problem due to the 2000–2014 global warming slowdown^{2–10} which occurred during a time of continuously increasing greenhouse gas (GHGs) concentrations. Both observational and modeling studies have explored potential mechanisms to explain this warming slowdown and concluded that internal decadal variability played a major role. The internally generated variability is associated with Pacific decadal variability (PDV, often associated with the Interdecadal Pacific Oscillation, IPO)^{11–19} and Atlantic multi-decadal variability (AMV, often associated with the Atlantic Multidecadal Oscillation, AMO).^{20–28} Additional contributions likely came from radiative cooling effects^{29–33} due to volcanic aerosols and consequent dimming of sunlight. Such decadal climate variability can lead to a redistribution of the heat absorbed by the climate system. For example, more energy can be transported into the subsurface and deep oceans instead of warming the upper few tens meters of ocean, thus contributing to a slowdown in global mean surface air temperature (GMSAT) increase.^{13,34–40} A linkage between the time-evolution of observed GMSAT and PDV has been established whereby there is a weaker GMSAT increase for PDV negative phase (with the tropical Pacific somewhat cooler than average on decadal timescales) and accelerated warming for PDV positive phase since the early 20th century.^{41,42}

However, these results may be affected by how the externally forced and the internally generated GMSAT changes are separated due to the fact that these factors work on the observed GMSAT simultaneously. Generally, the SAT trends over a century are dominated by external forcings; variability on timescales shorter

than a decade are more typically associated with natural variability. Variability between these two timescales is primarily the result of the interplay between the externally forced and internally generated changes.^{4,5,18,19,43–46} The simplest way to isolate the naturally occurring SAT changes from human-induced ones on both global and regional scales in observations is to remove the GMSAT linear trend. This is intended to represent the effects of the increase in GHGs, and is typically considered to be the anthropogenic climate change signal.⁴¹ But since the changes of anthropogenic forcing are not linear in time, this method inevitably leaks some human-induced changes into the residuals. Another commonly used method is based on climate model simulations, such as the externally forced GMSAT change as represented by a multi-model ensemble mean of 20th century climate model simulations.^{41,42} Averaging across the multi-model ensemble removes most of the randomly occurring internally generated variability, leaving the externally forced response including both the GHGs and natural forcings (solar and volcanoes). At the same time, other methods^{4,17,26–29,47–51} based on more complicated mathematics or statistics have been proposed to analyze time-varying GMSAT trends. Because none of these techniques has a direct physical connection to the time-evolution of the actual anthropogenic forcing, it is not surprising that these methods often produce inconsistent results. Here we propose a more physically consistent way to separate the influences of anthropogenic forcing and internal decadal variability by relating the forced GMSAT change in observations directly to changes of anthropogenic sources, and the residual GMSAT evolution to AMV and PDV.

¹Beijing Climate Center, China Meteorological Administration, No. 46, Zhongguancun South Street, 100081 Beijing, China; ²National Center for Atmospheric Research, PO Box 3000, Boulder, Colorado 80305, USA; ³University of Chinese Academy of Sciences, No. 19(A) Yuquan Road, 100049 Beijing, China; ⁴Chinese Academy of Meteorological Sciences, No. 46, Zhongguancun South Street, 100081 Beijing, China and ⁵China Meteorological Administration Training Centre, No. 46, Zhongguancun South Street, 100081 Beijing, China
Correspondence: Tongwen Wu (twwu@cma.gov.cn) or Aixue Hu (ahu@ucar.edu)

Received: 8 January 2019 Accepted: 21 May 2019

Published online: 11 June 2019

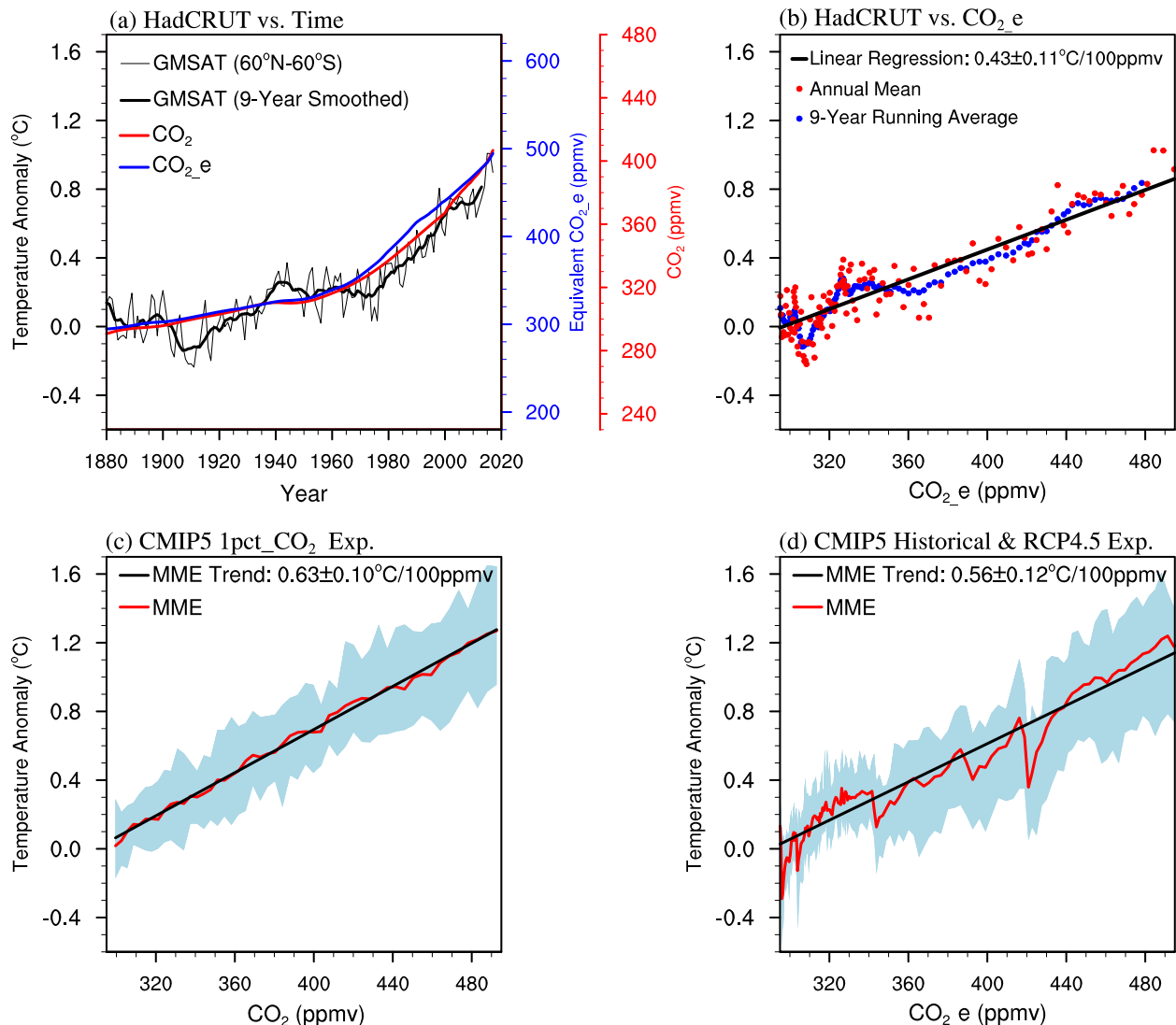


Fig. 1 Concentration of the atmospheric CO_2 and equivalent CO_2 , and observed and simulated global mean surface air temperature anomalies (GMSAT). GMSAT is defined as area-weighted man surface air temperature between 60°S and 60°N . **a** Annual-mean (thin black line) and its 9-year smoothed (thick black line) time series of GMSAT anomalies relative to the 1881–1910 mean derived from HadCRU data (Methods), and atmospheric CO_2 (red line) and equivalent CO_2 (CO_2 _e, blue line) concentrations. **b** Red and blue points denote the annual mean and its 9-year smoothed GMSAT change with CO_2 _e from 1880 to 2017, respectively. **c** CMIP5 1pct_ CO_2 experiment (Methods), and the GMSAT anomalies relative to the mean of the first 5 years run for each CMIP5 model. **d** CMIP5 historical from 1881 to 2005 and RCP4.5 experiments from 2006 to 2017 (Methods), and the reference climate is the mean of 1881 to 1910. Solid black Lines in **b**, **c**, **d** denote linear trend of 9-year smoothed GMSAT; red lines in **c** and **d** represent the ensemble mean GMSAT, and the shading represents the GMSAT spread of the 16 CMIP5 models

RESULTS

Global mean SAT change vs. GHGs

Figure 1a shows the annual mean (thin black line) and 9-year running mean (thick black line) of the area-weighted GMSAT between 60°S to 60°N from the Hadley Center Climate Research Unit (HadCRU) data version 4 from 1880 to 2017.⁵² The exclusion of polar-regions is due to the lack of long term reliable observations there (Supplementary Fig. 1). GMSAT rises more than 1°C in the last one and half centuries, half of which has been attributed to the increased GHG concentrations by many previous studies.^{18,48} To collectively consider the effects of well-mixed GHGs on GMSAT, we employ the concept of equivalent CO_2 (CO_2 _e hereafter) to include all well-mixed GHGs (e.g., CO_2 , CH_4 , NO_x , CFCs). To derive CO_2 _e, the observed time-evolving effective radiative forcing from each individual GHG source is summed up to get the total radiative forcing based on Intergovernmental

Panel on Climate Change (IPCC) 5th Assessment Report (AR5)⁵³ Table All.1.2, and then this total radiative forcing is converted into the concentration of CO_2 _e (see methods section for details). From 1881 to 2011, the observed CO_2 concentration increases by 99 parts per million by volume (ppmv; from 291 to 390 ppmv; red line in Fig. 1a), but CO_2 _e increases by 177 ppmv (from 295 to 472 ppmv; blue line in Fig. 1a). When GMSAT is plotted against CO_2 _e, the observed GMSAT changes almost linearly with CO_2 _e for both annual mean and 9-year running mean data with a rate of about $0.43 \pm 0.11^{\circ}\text{C}$ per 100 ppmv CO_2 _e (Fig. 1b). This linear relationship is more obvious when the CO_2 _e is above 350 ppmv (roughly after 1980 which might be related to the larger rate of CO_2 _e increase as shown in Supplementary Fig. 2), coincident with the rapid global warming period as shown in Fig. 1a. Before 1980, the large variations of the GMSAT imply that internal variability and natural external forcings (e.g., volcanoes) may have played a more important role in modulating GMSAT on decadal timescales, while

the changes in GHGs dominate centennial timescale trends. This will be discussed in more detail below.

To further verify this linear relationship, we analyze two sets of the Coupled Model Intercomparison Project phase 5 (CMIP5) experiments from 16 models.⁵⁴ These include the idealized experiment with one percent CO_2 increase per year compound (hereafter 1pct_CO₂) and the 20th century historical experiment from 1850 to 2005 with time-evolving natural and anthropogenic forcings (hereafter 20C). To extend the 20C experiment to 2017, the experiment using representative concentration pathway 4.5 (RCP4.5) is used. To be consistent with observations, GMSAT for the model simulations is also defined as an area-weighted mean between 60°S and 60°N. By using CO₂_e as in observations, the ensemble mean rate of GMSAT changes is $0.63 \pm 0.10^\circ\text{C}$ per 100 ppmv CO₂_e for 1pct_CO₂ runs and $0.56 \pm 0.12^\circ\text{C}$ per 100 ppmv CO₂_e for the 20 °C experiments (Fig. 1c, d). Although both of the GMSAT change rates are higher than the observed, the overestimation is statistically significant for the 1pct_CO₂ runs and insignificant for the 20 °C runs based on a student *t*-test, suggesting that the lack of aerosols in the 1pct_CO₂ runs likely contributes to this overestimation. In fact, this can be seen clearly by comparing the ensemble mean GMSAT changes in these two sets of model simulations with the ensemble mean GMSAT linear trend (red vs. black lines in Fig. 1c, d). Without the aerosols, these two lines are almost non-distinguishable (Fig. 1c); with aerosols, the GMSAT long-term linear trend departs significantly from the ensemble mean for certain time periods (Fig. 1d). It is worth noting that there is an overly strong response of the CMIP models to aerosol forcing, especially volcanic aerosols, in comparison to observations (Fig. 1b vs. d).⁵⁵ Nevertheless, our results indicate that the transient GMSAT changes on decadal or longer timescales for both observations and model simulations can be scaled linearly by changes of CO₂_e concentration.

To further test whether this relationship holds at regional scales, 12 grid points are randomly selected with 6 grid points over land and 6 points over ocean from observations. Results show that the same linear relationship between grid point temperature changes and CO₂_e generally holds well (Fig. 2), especially for the 9-year running mean data. The least square fit trends on the selected grid points are larger over land and smaller over ocean than the global mean, which is consistent with the overall greater land warming and less ocean warming due to the differences in heat capacity. The uncertainty varies from one grid point to another which is associated with the SAT variability on regional scales.

Definition of the decadal climate modes (AMV and PDV)

Because of the linear relationship between GMSAT and CO₂_e, the GHG-induced SAT changes can be derived by regressing CO₂_e onto global mean or regional SAT, or sea surface temperature (SST). With nonlinear changes of CO₂_e over the 20th century (Fig. 1a), the resulting nonlinear changes of regional SAT, GMSAT, and SST induced by CO₂_e (Supplementary Figs. 2 and 3) need to be properly removed in order to avoid the leakage of this signal into decadal climate mode variability. To derive the AMV and PDV indices, a rotated empirical orthogonal function (REOF) analysis is applied to the 9-year running mean SSTs in a domain that extends over both the Atlantic and Pacific basins between 40°S and 60°N after the removal of the CO₂_e-induced regional SST changes (see Methods section for details). The resulting REOF time series and spatial patterns are shown in Fig. 3. The REOF1 time series is almost identical to the more classic AMO defined as the area-weighted SSTs in the North Atlantic between equator and 60°N after the removal of the global mean SST time series⁵⁶ with a correlation coefficient of 0.80 (Fig. 2a blue and black lines). The REOF2 time series is nearly the same as a more typical IPO index defined as the first principle component (PC1) of the empirical orthogonal function (EOF) analysis for the Pacific basin after the

removal of the global mean trend^{11,12,57} with a correlation coefficient of 0.73 (red and orange lines in Fig. 3a). The spatial patterns of REOF1 and REOF2 resemble the spatial patterns of the AMO and IPO in their own basins, respectively (Fig. 3b, c), consistent with previous studies.^{56,57} But the connections to other basin differ a bit, especially for AMV, where there is a negative IPO-like pattern in the Pacific for the REOF1 pattern, and an AMO-like pattern in the Atlantic that is stronger than the classical AMO defined in⁵⁶ (Supplementary Fig. 4). This implies that the simple removal of the GMSAT time series will remove part of the AMV's contribution to the transient changes of GMSAT and regional SAT which further leads to an underestimation of the AMV influence on global and regional SAT changes. Connections to global climate must consider that there are contributions from both basins in this definition of AMV. Conversely, the PDV pattern is centered mostly in the Pacific with a classic IPO pattern, with only weak connections to the Atlantic. Therefore, most of the contributions to global climate from PDV defined in this way are from the Pacific basin. Hereafter, we define the REOF1 time series as AMV, and the REOF2 time series as PDV, and the corresponding spatial patterns as AMV and PDV patterns. This definition will be used throughout the following discussion and all data mentioned hereafter are the 9-year running mean data. The underlying assumption for using 9-year running mean data is that the linear relationship between SAT and CO₂_e is closer than that between annual mean SAT and CO₂_e as the climate needs time to equilibrate with the changes of CO₂_e forcing (or lagged response of the climate system to CO₂_e forcing).

A few recent studies^{25–28} pointed out the potential of mode mixing during the mode-deriving processes by using filtering. Here although we have applied an REOF technique to maximize the signals of AMV and PDV via analyzing the 9-year running mean data, the resulting AMV and PDV are negatively correlated with a correlation coefficient of -0.39 . This could result from mode mixing or maybe more physically represents an interaction between these two modes since they occur simultaneously in both observations and coupled model simulations. On decadal or longer timescales, the interaction between these two modes could possibly not be avoidable which needs to be studied further.

Contribution of GHGs and internally generated decadal climate variability to long-term global and hemispheric mean SAT changes
After the removal of the GHG-induced trend (blue line in Supplementary Fig. 3a), the residual GMSAT anomaly (red line in Supplementary Fig. 3a) exhibits significant multi-decadal timescale variability. This variability is highly correlated to AMV on centennial timescales, suggesting a more important role of AMV as defined above in contributing to observed GMSAT time-evolution along with the long-term trend contributed by anthropogenic forcings, in a good agreement with recent studies.^{26–29}

To further quantify this relationship, multiple linear regression is applied to the observed GMSAT and AMV, PDV and CO₂_e (Fig. 4). With the combined effects of these three factors, the observed 9-year running GMSAT is recovered at values over 99% (Fig. 4a). If only CO₂_e and AMV (or PDV) are used for the regression, the recovery of GMSAT is 98.7% (94.7%). As indicated in the methods section, there is no correlation between CO₂_e and AMV, or between CO₂_e and PDV, but the AMV and PDV are negatively correlated to each other. From the regression coefficients shown in the methods section, the changes of the regression coefficients when different modes are combined with CO₂_e are small for AMV, but large for PDV. This may imply that the overall contribution of AMV to the GMSAT changes in the last century-and-a-half is larger than the PDV's. Because of the use of standardized indices for CO₂_e, AMV and PDV, it is assessed that

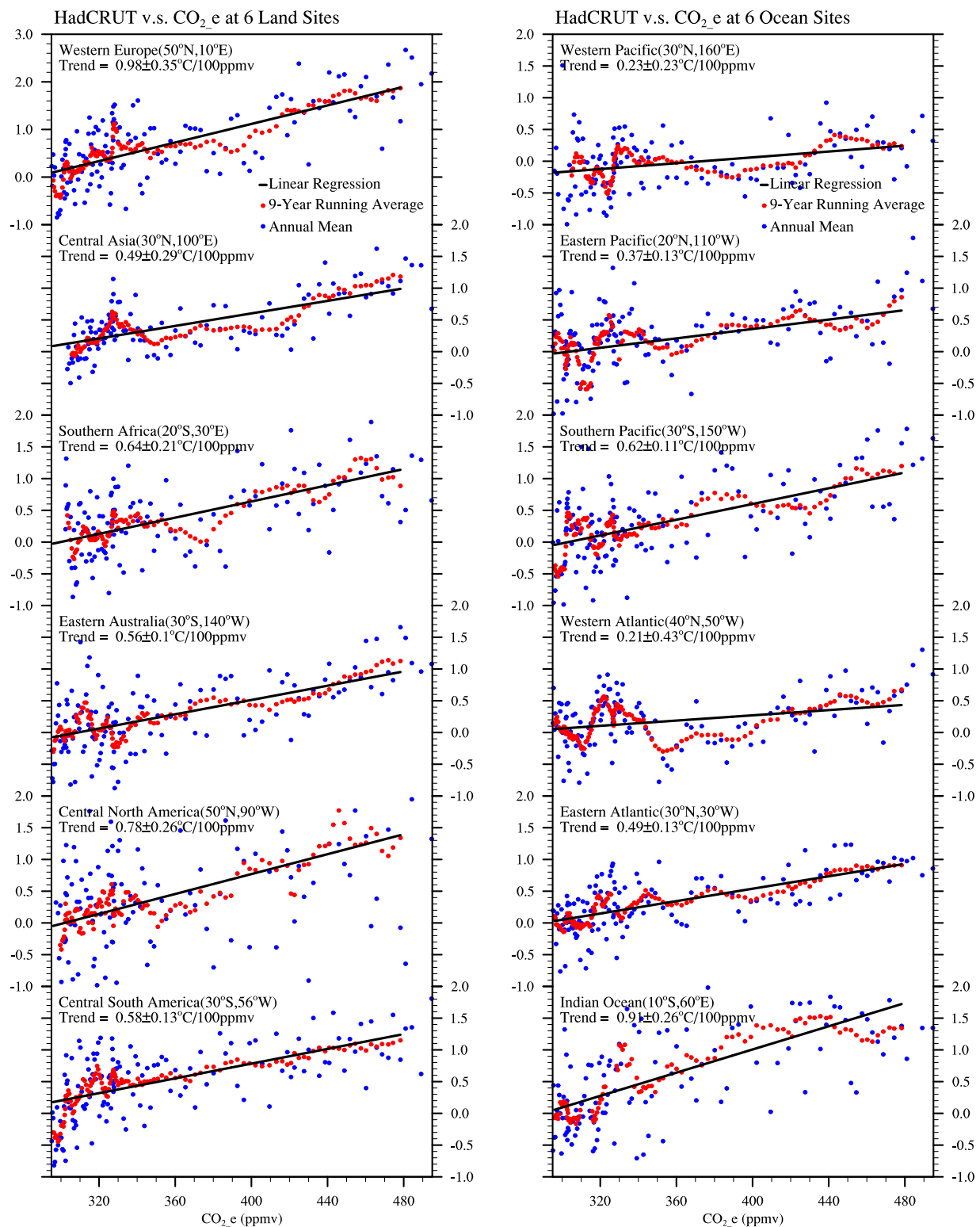


Fig. 2 Observed annual surface air temperature (SAT) anomalies and atmospheric equivalent CO_2 (CO_2 _e) concentrations. Here, 12 sites are randomly selected with 6 land sites (left panels) and 6 ocean sites (right panels). Red and blue points denote annual mean and its 9-year smoothed of SAT change with CO_2 _e from 1880 to 2017, respectively

the overall contribution from CO_2 _e to GMSAT changes is 70%, with 30% from AMV and PDV.

According to Fig. 1a, GMSAT should increase 0.76 °C at the rate of 0.43 °C/100ppmv (CO_2 _e) due to the change of CO_2 _e from 295 ppmv in 1881 to 472 ppmv in 2011. From our regression analyses

above, AMV, PDV can cause GMSAT variations of ± 0.24 °C and ± 0.09 °C in this period, respectively. Therefore, the observed GMSAT transient evolution on centennial or longer timescales is dominated by the CO_2 _e effect with significant modifications from climate variability on decadal and multi-decadal timescales.

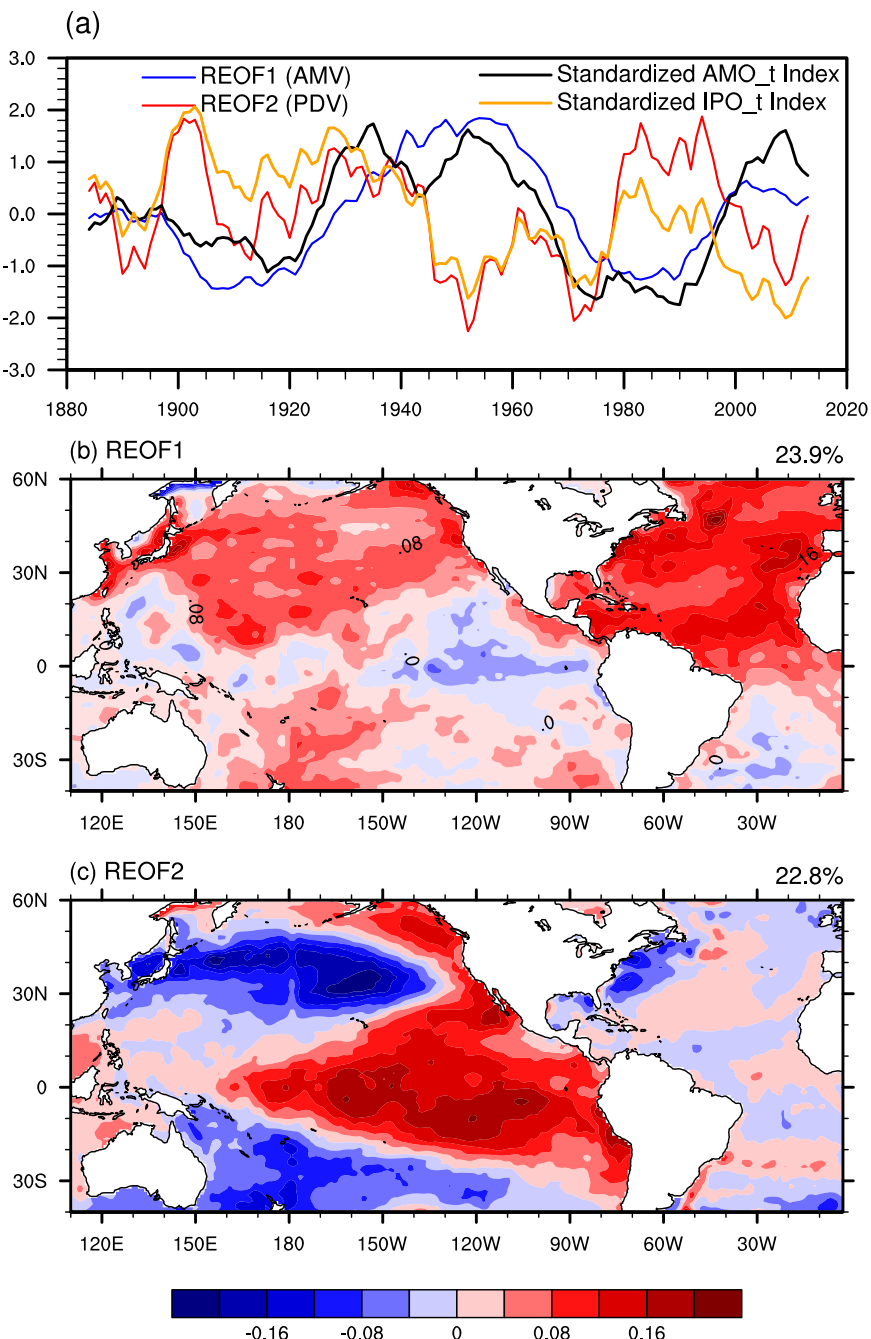


Fig. 3 AMV and PDV indices and their spatial patterns from Rotated Empirical Orthogonal Function (REOF) Analysis. The patterns is derived by regressing the AMV or PDV index on the residual of 9-year smoothed HadISST from 1881–2017 after CO_2 -induced effects are removed. Lines labeled REOF1 and REOF2 in panel **a** denote normalized AMV and PDV time series of the first two principal components. AMO_t index is the normalized AMO index based on ref. ⁵⁶. IPO_t is the IPO index derived based on ref. ⁵⁷ (Methods). Shading in **b** and **c** highlights the spatial pattern of REOF1 and REOF2. Numbers at the right top corner in **b** and **c** denote percent variance explained by REOF1 and REOF2 modes. Contour intervals for panels **b** and **c** are 0.04 °C per standard deviation of AMV or PDV

The contribution of $\text{CO}_2\text{-e}$ to hemispheric SAT changes in the recent century is larger in the Southern Hemisphere than in the Northern Hemisphere (80% vs. 64%, Fig. 4b, c). Correspondingly the combined contribution of the decadal climate modes to hemispheric SAT in the North is larger than that in the South (36% vs. 20%) with AMV being more important than PDV (Fig. 4b, c). It worth noting that the residual SAT in the Southern Hemisphere follows AMV well before 1940s, but there is a general cooling trend after the mid-1940s (Supplementary Fig. 3) which might

have contributed to the observed sea ice growth in the southern oceans⁵⁸ and needs to be studied further.

In comparison with previous studies^{13,14,17,37,41,42,59} that have pointed out the important role of PDV or decadal-timescale tropical Pacific SSTs in setting the pace of the observed GMSAT changes, here we show that AMV (with its contributions from the Pacific in this definition) could play a role in modulating this pace on multi-decadal or longer timescales, with PDV being more important on decadal timescales. The combination of $\text{CO}_2\text{-e}$ and AMV can reproduce the observed GMSAT better than the

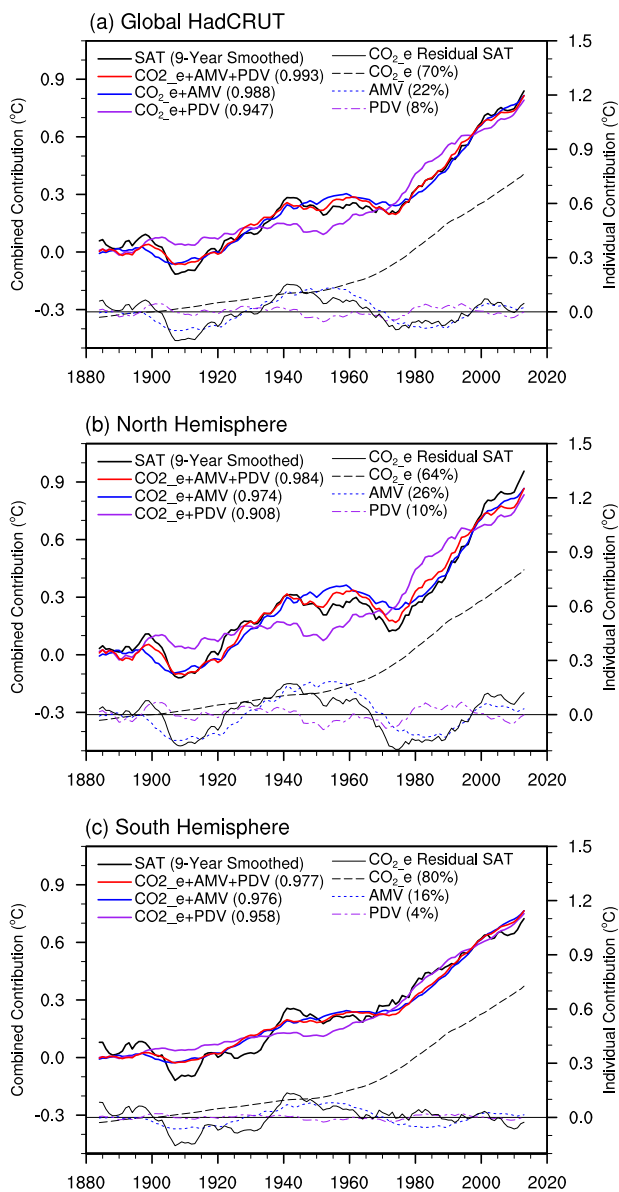


Fig. 4 Multiple linear regression of $\text{CO}_2\text{-e}$, AMV, PDV on global or hemispheric mean surface air temperature anomalies. The global or hemispheric mean surface air temperature anomalies is defined as area-weighted and 9-year running mean of global (60°S to 60°N) or hemispherical (60°S to equator or equator to 60°N) surface air temperature after the removal of $\text{CO}_2\text{-e}$ -induced temperature change. Solid black lines denote the time series of 9-year running mean SAT anomalies relative to the mean of 1881 to 1910, other color solid lines and the number in brackets at top left denote composited contributions of $\text{CO}_2\text{-e}$, AMV, and PDV to GMSAT and their correlation coefficients with 9-year running mean SAT. Dashed lines and numbers in brackets at top right denote the individual contribution of $\text{CO}_2\text{-e}$, AMV, PDV-induced SAT to GMSAT and the percentage of their individual contributions. Panel a is for the GMSAT, panels b and c are for the Northern and Southern Hemispheric SAT

combination of $\text{CO}_2\text{-e}$ and PDV for the last century and half. The latter combination overestimates the GMSAT changes for the periods 1900–1930 and 1972–1998, but underestimates those changes for the 1930–1972 and 1998–2013 periods with the former combination doing a much better job (Fig. 4). However, for the warming in the recent few years, the latter combination performs much better due mostly to the upward trending PDV

(Fig. 4) with a somewhat upward trend in enhanced $\text{CO}_2\text{-e}$ (Supplementary Fig. 2). Despite the strong relationship between GMSAT and AMV, the 21-year running lead-lag correlations show that most of the time PDV leads AMV by a few years regardless of whether they are positively or negatively correlated (Supplementary Fig. 5), suggesting that PDV could be playing a role in AMV (see more discussion in Method section). This might be the reason for realistically simulated GMSAT trends from specifying the tropical Pacific SSTs to observations.¹⁴ However, a few recent studies suggest that PDV may not contribute to the variability of the global mean climate much with the AMV dominating the multidecadal global mean climate variability.^{26–29} The discrepancy between our result and these few recent studies may be induced by the different methods to remove the GHG effect or due to the different methodology to derive the AMV and PDV which needs to be studied further.

A caveat in the discussions above is that the possible effect of aerosols on AMV^{60,61} was not removed. As shown in Supplementary Fig. 6, the removal of the global mean aerosol effect does not produce a major influence on the resulting AMV time evolution or its spatial patterns. However regional aerosol changes, such as over North America, Europe, and even Asia could potentially have some effect on AMV possibly after the 1940s (Supplementary Fig. 7, Supplementary Table 1). This is because the aerosol optical depth, a measure of the aerosol forcing in these regions, shows significant correlation with AMV after 1940s, but not with PDV. This might be causing changes in the relationship between PDV and AMV from a positive correlation before the 1930s to a mostly negatively correlation afterwards (Supplementary Fig. 5). This needs to be studied further (see Method for more discussion).

Contributions of GHGs and decadal climate modes to decadal GMSAT changes

To evaluate the contributions of GHGs and decadal climate modes (AMV and PDV) to decadal timescale GMSAT trends, the GMSAT is divided into sub-periods based on AMV/PDV phase transitions. Because of the different frequencies of PDV and AMV, the timing of their phase transitions is not the same. To compensate for these differences, the GMSAT was first sub-divided into four periods (Table 1) based on AMV phase transitions, then into 8 periods based on both PDV and AMV (Table 2). In general, the GHG-induced GMSAT trends are enhanced with an AMV/PDV phase transition from negative to positive, but weakened with an AMV/PDV phase transition from positive to negative. In-phase changes of AMV/PDV will make a larger contribution from decadal internal modes to GMSAT trends, and vice versa for out-of-phase changes.

As shown in Table 1, the AMV's contribution to GMSAT trends is significantly larger than the GHGs' contribution during the first AMV phase transition (1910–1941), is similar in magnitude for the second AMV phase transition (1942–1974), and is significantly smaller than GHGs' in the last two AMV phase transitions (1975–1999 and 2000–2013). The increasing contributions from GHGs over the 20th century are related to the accelerated rate of $\text{CO}_2\text{-e}$ changes, which varies from about 0.5 ppmv per year before 1945 to up to 3 ppmv per year after 1945 (Supplementary Fig. 2). This suggests that as the rate of GHG increase is continuously rising, the influence of AMV/PDV on GMSAT could become gradually less significant, agreeing with a previous study that examined the influence of PDV on future climate.⁶² For example, the contribution of GHGs to the GMSAT trend is two to three times larger than that from AMV and PDV for the recent two AMV phase transitions, but is much less for the earlier two AMV phase transitions.

However, when contributions from both AMV and PDV are considered in the GMSAT time series, the contribution of PDV to GMSAT trends is a similar magnitude to the AMV's contribution, or even larger, in certain periods (Table 2). There are four periods

Table 1. Trends of area-averaged global mean SAT based on AMV phase changes and contributions from anthropogenic forcing and nature variability

Periods	SAT trend (°C per decade)					AMV-index trend (per year)	PDV-index trend (per year)
	9-year smoothed	CO ₂ _e-induced	The residual	AMV-induced	PDV-induced		
1910–1941	0.110	0.025	0.085	0.069	0.012	0.096	0.050
1942–1974	−0.014	0.051	−0.065	−0.048	−0.006	−0.067	−0.025
1975–1999	0.166	0.130	0.036	0.034	0.013	0.047	0.053
2000–2013	0.089	0.125	−0.035	−0.019	−0.013	−0.026	−0.052

Note: statistics represent changes in 9-year smoothed HadCRUT anomalies relative to reference period of 1961 to 1990. TAS residual denotes the CO₂_e-induced SAT. Trends of AMV-induced and PDV-induced SAT are calculated for global SAT anomalies that had contributions from AMV and PDV variations (shown in Fig. 3)

with in-phase changes of PDV and AMV, and out-of-phase changes in the other four periods. The GMSAT trends from the in-phase PDV/AMV are larger than GHG-induced GMSAT trends, especially in the early 20th century. For the most recent period (2010–2013), the much faster warming contribution from PDV makes up about 1/3 of the warming with 43% from GHGs and only 8% from AMV. Out-of-phase PDV/AMV results in a much smaller contribution to the GMSAT trends from the decadal internal modes than from GHGs. For the periods 1953–1990 and 1991–2009, the combined contribution of PDV and AMV to the GMSAT trends is less than 50% compared to that from GHGs alone. Nevertheless, both PDV and AMV are capable of significantly modulating the GMSAT time evolution on decadal timescales and the strength of this modulation depends on whether their changes are in-phase or out-phase.

Contributions of GHGs and decadal climate modes to decadal regional SAT changes

To further study the contributions of the GHGs, AMV, and PDV to regional SAT changes, CO₂_e is regressed onto the regional SAT, while AMV and PDV are regressed onto the SAT residual (Fig. 5 and Supplementary Fig. 8). It is not surprising that the GHG-induced SAT increase is generally larger over land than ocean (Fig. 5a). The interior land areas of Eurasia and North America, especially the arid-areas and semiarid-areas from central Asia to northern China and Mongolia, are the regions where SAT warming is most sensitive to GHG increases compared to other regions of the globe. The regression patterns of AMV and PDV in Figs. 5b, 4c are similar to the patterns in Fig. 3b, c. That is, positive AMV is related to a warmer SAT in most regions except the southern oceans, parts of subtropical South Atlantic and equatorial Pacific, and parts of central Asia, India and the Southeast Asian peninsula, a fraction of equatorial Africa, and South America. The remote influence of AMV is suggested to be caused by the AMV excited circumglobal waves which propagate the North Atlantic SST anomaly signal through an atmospheric bridge into the Pacific and Indian Oceans^{63–66} and by ocean circulation changes in the South Atlantic.⁶⁷ For PDV, warmer SAT appears in most parts of the globe too, except the subtropical Pacific, the Atlantic and Indian sectors of the Southern Ocean, and parts of Europe. The multiple linear regression suggests a recovery of more than 80% of the observed regional SAT in most areas, implying that these three factors have played a dominant role in determining not only the variability and change of SAT on the scale of global mean, but also on the regional scales.

On the decadal timescale, we discuss two periods: 1953–1990 and 1991–2010. In the first, AMV is trending towards negative, but PDV is trending towards positive, and vice versa for the second period. As shown in Fig. 6a, b, the SAT trends resemble the PDV pattern in the Pacific, but AMV pattern in the Atlantic. The contribution of GHGs to the regional SAT trends is very similar for

these two periods but slightly larger for the second period. After removing the GHG-induced warming, the residual SAT trends show a weak positive PDV pattern in the Pacific and a strong negative AMV pattern in the Atlantic in the first period, but a strong negative PDV pattern in the Pacific and a strong positive AMV pattern in the Atlantic for the latter period. The magnitude of the PDV and AMV-related regional SAT trends is in general much larger than GHG-induced trends, suggesting that on regional scales, the decadal internal modes play a more dominant role in determining the local SAT trends. But on the global scale, the contributions of PDV and AMV to SAT trends tend to cancel each other out, leaving GHGs to be the dominant factor.

Projection of future SAT

The AMV and PDV defined in this study have some of the same characteristics as definitions in previous studies^{56,57} and have dominant multi-decadal timescale variability with a period about 50–80 years for AMV^{43,68} and 30–50 years for PDV.⁶⁹ As shown in Fig. 3a, AMV appears to be entering a transition from positive to negative phase since 2005, and PDV is transitioning to a positive phase after 2010. This out-of-phase change of AMV and PDV would minimize their combined influence on SAT, leaving the GHGs to be the dominant factor determining the SAT trends in the next couple of decades if the current tendency of the AMV and PDV does not change. If CO₂_e keeps the present rate of increase of about 3 ppmv per year (Supplementary Fig. 2), we can project the future regional SAT trend based on the linear relationship of CO₂_e and SAT. Figure 7 shows the two standard deviation values of regional residual SAT (panel a) and its ratio with the projected SAT warming due to increased GHGs, where a value greater than one represents the 95% significance level (panel b). In general, the warming on land is statistically significant on the multi-decadal timescale, but insignificant over most ocean regions. In other words, the internal variability induced by AMV/PDV could overcome the GHG-induced warming in southeastern China, the Southeast United States, parts of South America and Africa, most parts of the Pacific, North Atlantic, and the Southern Ocean on this timescale, but not in other parts of the world on decadal timescales (Fig. 7b).

A caveat for this projection is that as discussed in the method section and shown in Supplementary Fig. 12, the linear relationship between SAT and CO₂_e found here could break down for a rapid rise of the CO₂_e where the logarithmic fit could be a better choice. Although we have used a 9-year running mean data to consider the lagged response of the SAT to changes of CO₂_e, with a potentially much more rapid changes in CO₂_e in the future climate, our projected changes of SAT due to CO₂_e for the next few decades could be overestimated.

Table 2. Trends of area-averaged global mean SAT and contributions from anthropogenic forcing and nature variability

Periods	SAT trend (°C per decade)					AMV index trend (per year)	PDV index trend (per year)
	9-year smoothed	CO ₂ -e-induced	The residual	AMV-induced	PDV-induced		
1900–1912	−0.153	0.024	−0.177	−0.045	−0.062	−0.063	−0.253
1913–1927	0.118	0.025	0.093	0.054	0.020	0.075	0.083
1928–1952*	0.070	0.020	0.050	0.055	−0.031	0.076	−0.126
1953–1960*	0.056	0.101	−0.045	−0.074	0.017	−0.036	0.153
1961–1970	−0.036	0.071	−0.108	−0.111	−0.033	−0.155	−0.136
1971–1990*	0.147	0.136	0.012	−0.029	0.049	−0.040	0.200
1991–2009*	0.163	0.115	0.048	0.055	−0.039	0.077	−0.159
2010–2013	0.313	0.136	0.176	0.026	0.101	0.036	0.412

Note: The first column marked by “*” denotes the period when the AMV and PDV indices show opposite trends. The global mean SAT is defined as the area-weighted mean of SAT between 60°S and 60°N. The anthropogenic forcing is represented as CO₂-e, and the nature variability is represented by AMV and PDV

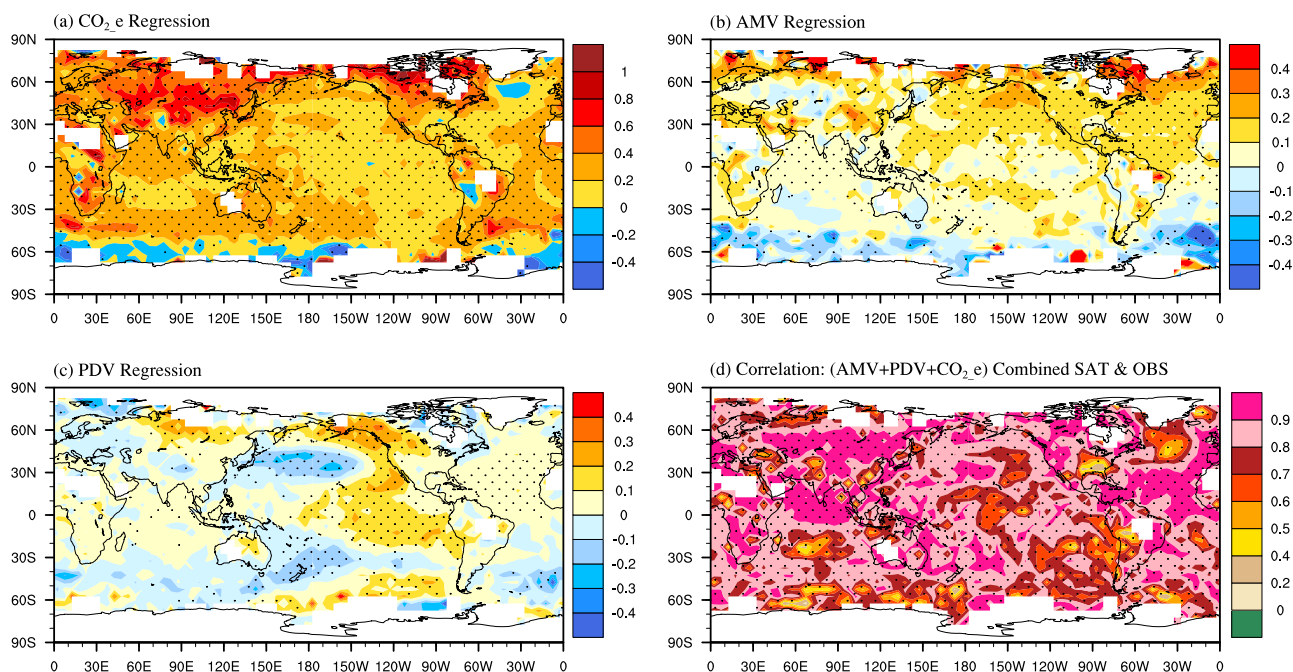


Fig. 5 Multi-regression coefficients of 9-year smoothed SAT with standardized CO₂-e, AMV and PDV indices, and correlation. **a–c** denote regression coefficients for CO₂-e, AMV, PDV. **d** denotes that the correlation coefficient between the combined SAT of CO₂-e, AMV, PDV-induced and the 9-year smoothed SAT. Values significant at the 99% level using a Student's t-test are stippled. The contour intervals are 0.2 °C per 100 ppmv CO₂-e for panel **a**, 0.1 °C per standard deviation of AMV (panel **b**) or PDV (panel **c**), and 0.2 for panel **d** (unitless)

DISCUSSION

Here by combining both observations and model simulation, we study how the interplay of anthropogenic climate change and internally generated decadal climate variability would determine the transient global and regional surface temperature changes. It is found that the GHG-induced SAT changes can be linearly scaled by the GHG change. Defined as the combined variability in the Atlantic and Pacific basins after the removal of GHG-induced SAT changes, both AMV and PDV play a significant role in modulating global mean and regional SAT changes in the past a century-and-a-half. Regression analysis indicates that the observed global mean SAT changes from 1880 to 2017 come 70% from contributions from GHGs, with AMV and PDV contributing a combined 30% with a possible higher contribution from AMV. Overall, the AMV contributes significantly to the global mean SAT transient changes on multidecadal timescale, however, the contributions of PDV and AMV to global mean SAT have similar

magnitudes on decadal timescales with the PDV leading AMV in most parts of the 20th century. Moreover, when PDV and AMV are in-phase, the contribution of natural decadal variability to global and regional climate can be significantly larger than that from GHGs, but an out-of-phase change of PDV and AMV could minimize their contribution to global and regional climate. As the GHGs increase further, our study shows a declined influence of the PDV and AMV to global and regional climate relative to that of GHGs.

By assuming a constant rate of GHG increase in next few decades, our analysis indicates that the GHG-induced warming will dominate the internal decadal-timescale variability in most land regions except southeastern China and North America where a less than global mean warming is likely to be experienced due to natural decadal variability. Further, in most ocean regions, AMV and PDV can still insert significant influence, resulting in large uncertainty on projecting the SAT changes there.

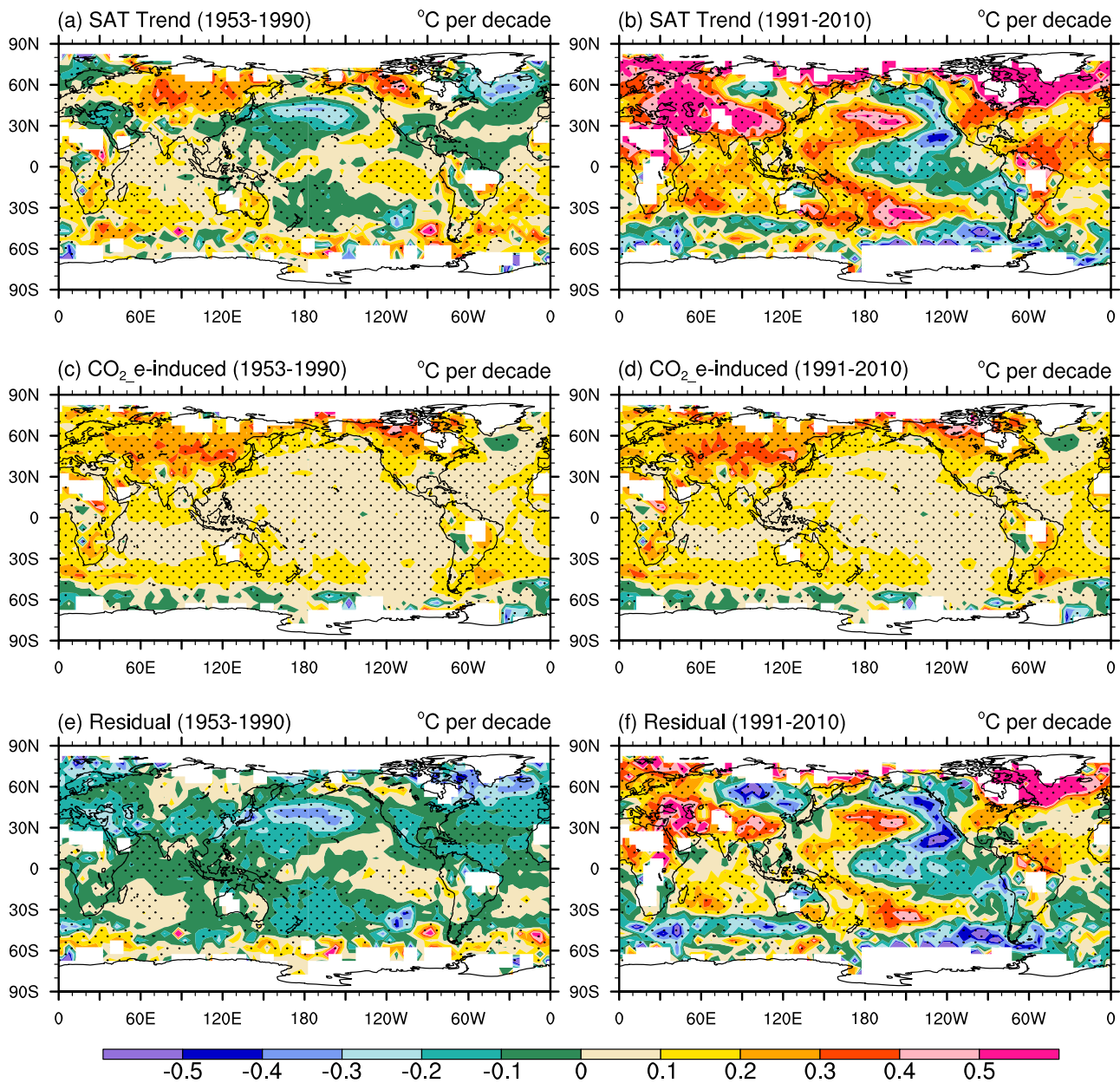


Fig. 6 Linear trends of SAT and the SAT trend contributed by $\text{CO}_2\text{-e}$, AMV and PDV. **a, b** Linear trends of 9-year smoothed gridded annual SAT anomalies during the period of 1953 to 1990, and 1991 to 2010, respectively. **c, d** $\text{CO}_2\text{-e}$ -induced SAT trends. **e, f** Residual SAT trends associated with AMV. Stippling indicates the 95% statistical confidence using a Student's *t*-test. The contour interval is 0.1°C per decade

It is worth pointing out that to derive AMV and PDV, the only externally forced response being removed is due to $\text{CO}_2\text{-e}$. Effects from other external forcings, such as solar and volcanoes, are still within the residual SAT data. Thus our method is significantly different from the method which uses the multi-model ensemble mean to represent the forced changes.^{41,42} This is because the forced trend, represented by the multi-model ensemble mean GMSAT, includes both anthropogenically and naturally forced components, and the trend removed in this study includes only the GHG component. The difference between these two trends should be the naturally forced component which could affect the AMV and PDV examined here. Certain differences from this study and previous studies on the contribution of AMV and PDV to GMSAT and the spatial patterns of AMV and PDV could rise from these different methodologies used to remove the forced trend. The motivation for us to keep the solar and volcano effects in the residual SAT is that the natural forcing is an integral part of natural

variability. The climate indices, including AMV and PDV, derived from proxy data do not exclude the effect of the natural forcing. To do a fair comparison of the climate indices derived from modern observations and proxy data, it is necessary to keep the natural forcing effect within the analyzed data.

METHODS

Gridded observational data sets

We primarily used the Hadley Centre–Climate Research Unit combined land surface air temperature and sea surface temperature (HadCRUT4) version 4.6.0.0 (<https://www.metoffice.gov.uk/hadobs/hadcrut4/>). HadCRUT4 is a $5^\circ\text{lon} \times 5^\circ\text{lat}$ gridded dataset of the observed global historical monthly surface temperature anomalies (relative to a 1961–1990 reference period) from 1850 to 2017, neither interpolated nor variance adjusted⁵². The SST of HadCRUT4 is based on HadSST3 (version HadSST3.1.1.0) which is a dataset of global monthly sea surface temperature anomalies

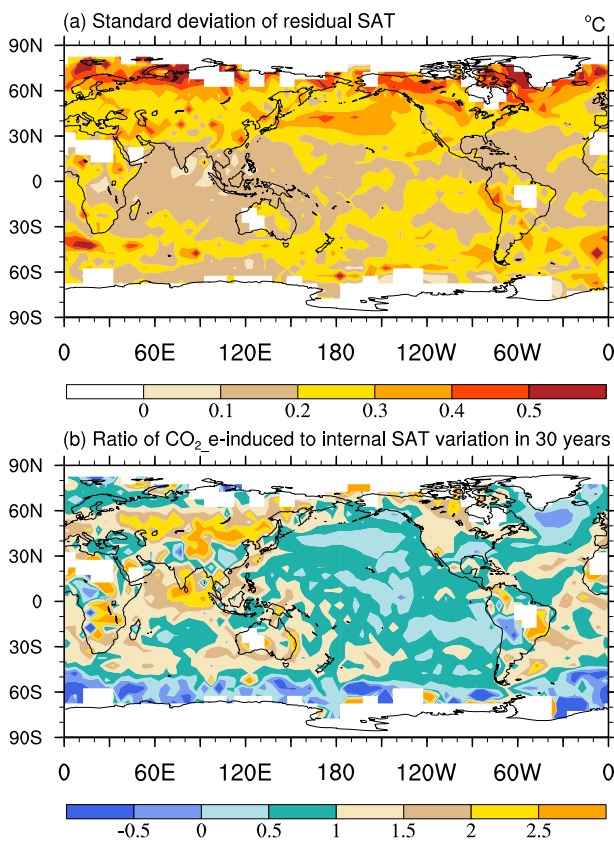


Fig. 7 Internal variations of SAT and its relative importance to CO₂_e-induced SAT. **a** The standard deviation of residual SAT of 9-year running annual mean HadCRU SAT anomalies from 1881 to 2017 computed by removing CO₂_e-induced SAT from the total SAT. **b** Ratio between GHG-induced SAT changes due to assumed 90 ppmv CO₂_e increase in the next 30 years and the two-standard deviation of residual SAT

produced by taking in-situ measurements of SST from ships and buoys, rejecting measurements that fail quality checks, converting the measurements to anomalies by subtracting climatological values from the measurements, and calculating a robust average of the resulting anomalies on a 5° by 5° grid.^{70,71}

To test the observed data set uncertainty, we also analyzed a widely used global 2° × 2° grid National Aeronautics and Space Administration (NASA) Goddard Institute for Space Studies (GISS) Surface Temperature Analysis dataset from 1881 to 2017,^{72,73} which covers most regions of the globe by sampling at the station level for land, and using ship-based and satellite-based measurements for ocean (<https://data.giss.nasa.gov/gistemp/>). A figure similar to Fig. 1 is shown in Supplementary Fig. 9. The results from the GISS data set are mostly consistent with HadCRUT data.

To derive the climate indices of AMV and PDV, we also used the objectively interpolated HadISST at 1 × 1 degree horizontal resolution⁷⁴ in order to avoid the influence of missing data on the resulting AMV and PDV indices and spatial patterns (<https://www.metoffice.gov.uk/hadobs/hadisst/>).

Global HadCRUT annual mean estimates and 9-year smoothing

As shown in Supplementary Fig. 1, the spatial and temporal coverage of the SAT observations is not uniform, especially before the 1920s, and in regions poleward of 60°. To get a better spatial and temporal coverage, the global gridded annual mean HadCRUT data were calculated for grid boxes where data are available for more than 67% of year i.e., at least eight months per year. Regions poleward of 60° are excluded from our calculation due to the significant lack of observed samples. Then, 9-year

smoothed SAT values are calculated for annual mean data using an unweighted running-time mean.

CMIP5 models data sets

Simulations of 16 models from the Coupled Model Intercomparison Project phase 5 (CMIP5)⁵⁴ were used (ACCESS1-3, BCC-CSM1-1, BCC-CSM1-1m, CanESM2, CCSM4, CNRM-CM5, CSIRO-Mk3-6-0, FGOALS-g2, GFDL-CM3, GISS-E2-R, HadGEM2-AO, IPSL-CM5A-MR, MIROC5, MPI-ESM-MR, MRI-CGCM3, NorESM1-M). Idealized 1pct_CO₂ and historical experiments from 1850 to 2005 and representative concentration pathway 4.5 (RCP4.5)⁷⁵ experiments from 2006 to 2017 (20C hereafter) were used.

The 1pct_CO₂ experiment is a common standardized forcing scenario that specifies atmospheric CO₂ to increase at a rate of 1%/year compound from a model initial state at the level of 285 ppmv CO₂ in 1850 AD until the concentration doubles at model year 70 (or quadruples at model year 140) and is then held constant. These runs reach the present equivalent CO₂ (CO₂_e) concentration—estimated to be 494.6 ppmv in 2017 using expression (2)—at year 55 in the 1pct_CO₂ experiment (observed CO₂ concentration around this time is about 400 ppmv; see next section for the definition of CO₂_e concentration). Therefore, only the first 55 years of 1pct_CO₂ experiments are analyzed in Fig. 1c.

The 20C experiments are run from 1850 to 2005 with time-evolving anthropogenic (e.g., CO₂, CH₄, NO_x, O₃, etc.) and natural forcings (solar and volcanic aerosols). To extend the model data to 2017, the RCP4.5 scenario is used from 2006 to 2017. The RCP4.5 scenario is considered to be a medium level scenario for anthropogenic GHG emissions.⁷⁵ In Fig. 1d, the CO₂_e concentrations from 1881 to 2005 are observed, but those from 2006 to 2017 are estimated from the CO₂ concentrations that are used in RCP4.5 in the same period, and then converting them to CO₂_e concentrations by applying expression (2) below.

CO₂ and CO₂_e data sets

The observed atmospheric CO₂, a major greenhouse house gas (GHG), increases from 290 parts per million by volume (ppmv) in 1881 to 404 ppmv in 2017. (Fig. 1a, https://www.esrl.noaa.gov/gmd/ccgg/trends/global.html#global_data). When the global mean surface air temperature (GMSAT) changes are plotted against the changes of CO₂ concentration (Supplementary Fig. 10), we find a linear relationship between the transient HadCRU GMSAT variations and CO₂ with a mean rate of change $0.83 \pm 0.07^\circ\text{C}$ per 100 ppmv CO₂ for period 1880–2017 (Supplementary Fig. 10a). A linear relationship between GMSAT and CO₂ is also found in the 1pct_CO₂ and 20C experiments from all CMIP5 models with an ensemble mean warming rate of $0.66 \pm 0.11^\circ\text{C}$ per 100 ppmv CO₂ for the former (Supplementary Fig. 10b) and $1.04 \pm 0.23^\circ\text{C}$ per 100 ppmv CO₂ for the latter (Supplementary Fig. 10c). Apparently, the 1pct_CO₂ experiments underestimate the observed warming rate, while there is an overestimation in the 20C experiments. Since the observed GHGs include not only CO₂, but also methane (CH₄), ozone (O₃), nitrous oxide (NO_x), chlorofluorocarbons (CFCs), etc., the different simulated rate of GMSAT changes in these two sets of experiments is likely due to the difference in forcings, such that the 1pct_CO₂ experiments include only CO₂, but all known anthropogenic forcings as while as the natural forcings are included in the 20C experiments.

To reconcile the differences in these two sets of CMIP5 experiments and the differences between CMIP5 simulations and observations, we employ the concept of equivalent CO₂ (CO₂_e hereafter) to include all well mixed-GHGs (e.g., CO₂, CH₄, NO_x, CFCs). To derive CO₂_e, the observed time-evolving effective radiative forcing from each individual GHG source is summed up to get the total radiative forcing based on the Intergovernmental Panel on Climate Change (IPCC) 5th Assessment Report (AR5) Table All.1.2⁵³, and then this total radiative forcing is converted into the concentration of CO₂_e as outlined below.

The observational data of atmospheric CO₂ concentration from 1851 to 2005 are the CMIP5-recommended global CO₂ observation data set. The global averaged CO₂ data from 2006 to 2017 are downloaded from https://www.esrl.noaa.gov/gmd/ccgg/trends/global.html#global_data. Equivalent CO₂ (CO₂_e) in this work is defined as the amount of CO₂ used in a model calculation that results in the same radiative forcing of the surface-troposphere system as that caused by all well-mixed Greenhouse Gases (WMGHG) including CO₂. The time series of annual CO₂_e from 1881 to 2011 is calculated using the expression to convert from historical WMGHG

effective radiative forcing (*ERF*) based on the Fifth Assessment Report (AR5) Table All.1.2,

$$\text{CO}_2\text{-e} = \text{CO}_2\text{-orig} \cdot e^{\frac{\text{ERF}}{35}}, \quad (1)$$

where $\text{CO}_2\text{-orig}$ is 278 ppmv in year 1750 and *ERF* (in Wm^{-2}) is relative to a zero baseline in year 1750 and represents additional forcing compared with pre-industrial levels. The $\text{CO}_2\text{-e}$ data in the period from 2012 to 2017 were estimated using a highly linear correlation relationship between CO_2 and $\text{CO}_2\text{-e}$ during the period of 1991 to 2011 (Supplementary Fig. 11),

$$\text{CO}_2\text{-e} = \text{CO}_2 \cdot 1.46 - 98.60. \quad (2)$$

From 1881 to 2011, the observed CO_2 concentration increases by 99 ppmv (from 291 to 390 ppmv; Fig. 1a red line), but $\text{CO}_2\text{-e}$ increases by 177 ppmv (from 295 to 472 ppmv; Fig. 1a blue line).

Trend estimates

The trend of HadCRU SAT variations during the period from 1881 to 2017 with atmospheric $\text{CO}_2\text{-e}$ concentration in Fig. 1b was calculated using a linear regression and its statistical uncertainty is calculated as the standard deviation of running trends in a 100 ppmv $\text{CO}_2\text{-e}$ window. The trend of ensemble CMIP5-model SAT variations with CO_2 concentration in Fig. 1c and $\text{CO}_2\text{-e}$ concentration in Fig. 1d are calculated using global (60°S to 60°N) annual mean surface air temperature from 16 CMIP5 climate models⁵⁴ for the historical forcing from year 1880 until 2005 and followed by the RCP4.5 scenario to year 2017. Its statistical uncertainty in Fig. 1c, d is calculated as the standard deviation of 16 CMIP5 simulated trends.

Would the linear relationship between $\text{CO}_2\text{-e}$ and GMSAT hold for much larger changes in $\text{CO}_2\text{-e}$? To answer this question, the full length of the 1pct_ CO_2 experiment is analyzed. As mentioned earlier, the $\text{CO}_2\text{-e}$ in the full length of the 1pct_ CO_2 experiment changes from 285 ppmv to 1140 ppmv. As shown in Supplementary Fig. 12, the linear relationship between $\text{CO}_2\text{-e}$ and GMSAT performs better than a logarithmic fit for a smaller change of $\text{CO}_2\text{-e}$, such as a change of $\text{CO}_2\text{-e}$ less than 200–300 ppmv which is the case in this study (top panel in Supplementary Fig. 12). However, for a much larger change of $\text{CO}_2\text{-e}$, the linear fit may not be the best, and the logarithmic fit or another nonlinear fit may perform better. In reality, $\text{CO}_2\text{-e}$ changes that occur in a period of less than a century may not be significantly larger than 300 ppmv. Therefore, in most cases, for climate changes on decadal or multi-decadal timescales, the linear fit between $\text{CO}_2\text{-e}$ and GMSAT is a good approximation for the GHG-induced global and regional SAT changes.

Definition of AMV and PDV index

AMV index is commonly derived by subtracting the global (60°N – 60°S) mean SST time series from the area-weighted North Atlantic mean SST time series⁵⁶ or the linear detrended North Atlantic SST⁴⁵. The PDV index is traditionally defined as either the second empirical orthogonal function (EOF) of low-pass filtered Pacific basin SSTs (the first EOF being the trend), or the first principle component (PC1) of the EOF analysis after removing the global mean trend.⁵⁷ Another option for defining the PDV is to use the tripole PDV Index based on the difference between the SSTA averaged over the central equatorial Pacific and the average of the SSTA in the Northwest and Southwest Pacific.⁷⁶ In this study, AMV and PDV indices are defined as the time series of the first and the second leading components of the REOF analysis for residual SSTA after removing the $\text{CO}_2\text{-e}$ -induced regional SSTA changes over Pacific and Atlantic regions between 110°E to 0° and between 40°S to 60°N . Therefore, these definitions of AMV and PDV differ from the previous AMV^{20,21} and PDV^{11,12} definitions since there are connections between ocean basins that are captured here in the EOFs that use the entire Atlantic and Pacific domains together.

Though the AMV and PDV indices defined in this research are not the same as the more traditionally defined AMV and PDV indices, the respective spatial patterns do resemble features of the traditional AMV and PDV (Fig. 2 and Supplementary Fig. 4). However, the 21-year running lead-lag correlations between PDV and AMV show significant differences between these two indices and those for PDV and AMV defined in more traditional ways (Supplementary Fig. 5). For example, the PDV almost always leads the AMV by a few years for the indices defined in this research, but the relationship is mixed for the more traditionally defined PDV and AMV. This consistent relationship between PDV and AMV defined here may indicate that the PDV may have an influence on the AMV when both ocean basins are used to compute the indices. Potentially this may give us a clue as to why, when specifying realistic tropical Pacific SST

variability, the work of Kosaka and Xie¹⁴ shows that a partially coupled model was able to simulate the observed GMSAT time evolution.

Previous research⁷⁷ also shows that anthropogenic aerosols may have influenced the AMV. From Supplementary Table 1 and Supplementary Fig. 7, the changes of anthropogenic aerosols are small before the 1940s, but significantly increase after the 1940s until the 1980s, then reduce dramatically afterwards in the North American and European regions. In other regions, these aerosols increase all the way to the early 2000s with varying rates. The correlation between the AMV and the aerosol optical depth (AOD) in both North America and Europe show a consistently negative correlation since the 1940s. However, the correlations between the AMV and East Asian and South Asian climate are not as consistent. For example, although their correlations are negative after the 1940s, they become positive after the 1980s. This may suggest that Asian aerosols do not affect Atlantic SST variability much, but the aerosols in North America and Europe may have played a role in modulating Atlantic SST variability only after the 1940s. This would call into question whether the aerosols really affected the AMV or was it just a coincidence? Is the aerosol forcing too weak before the 1940s to influence the AMV? These questions require further study.

On the other hand, the effect of aerosols on the PDV is minimal which can be clearly seen from Supplementary Table 1. The correlation coefficient between AOD and PDV is very small for all regions, but increases significantly after the 1980s due to the rising trend of AOD in Asia and the decreasing trend of AOD in North America and Europe, which are coincident with an overall downward trending PDV. Thus it may be safe to say that there is no significant impact of aerosols on PDV variability.

Individual contributions of $\text{CO}_2\text{-e}$, AMV, PDV-induced SAT to global or hemispheric SAT variations

Area-weighted 9-year running means of global or hemispheric surface air temperature (SAT) anomalies from 1881 to 2017 are regressed onto the normalized time series of $\text{CO}_2\text{-e}$, AMV and PDV indices using multiple linear regression. By using these standardized indices, their regression coefficients can be interpreted as the strength of individual contributions of $\text{CO}_2\text{-e}$, AMV and PDV-induced SAT to global or hemispheric SAT variations. The percentages of individual contributions to global or hemispheric SAT variations in Fig. 3 are estimated using ratio values of each regression coefficient to their sums. The regression equations are listed below:

$$\text{GMSAT} = 0.229 \times \text{CO}_2\text{-e} + 0.072 \times \text{AMV} + 0.024 \times \text{PDV} \quad (3)$$

$$\text{GMSAT} = 0.229 \times \text{CO}_2\text{-e} + 0.062 \times \text{AMV} \quad (4)$$

$$\text{GMSAT} = 0.229 \times \text{CO}_2\text{-e} - 0.004 \times \text{PDV} \quad (5)$$

$$\text{NHSAT} = 0.241 \times \text{CO}_2\text{-e} + 0.099 \times \text{AMV} + 0.037 \times \text{PDV} \quad (6)$$

$$\text{NHSAT} = 0.241 \times \text{CO}_2\text{-e} + 0.084 \times \text{AMV} \quad (7)$$

$$\text{NHSAT} = 0.241 \times \text{CO}_2\text{-e} - 0.002 \times \text{PDV} \quad (8)$$

$$\text{SHSAT} = 0.218 \times \text{CO}_2\text{-e} + 0.044 \times \text{AMV} + 0.011 \times \text{PDV} \quad (9)$$

$$\text{SHSAT} = 0.218 \times \text{CO}_2\text{-e} + 0.040 \times \text{AMV} \quad (10)$$

$$\text{SHSAT} = 0.218 \times \text{CO}_2\text{-e} - 0.006 \times \text{PDV} \quad (11)$$

Where GMSAT, NHSAT, and SHSAT represent the 9-year running global mean, Northern Hemisphere mean and Southern Hemisphere mean surface air temperature, respectively. $\text{CO}_2\text{-e}$, AMV, and PDV represent the standardized indices of $\text{CO}_2\text{-e}$, AMV, and PDV.

The correlations between these indices show that there is no correlation between $\text{CO}_2\text{-e}$ and AMV, or $\text{CO}_2\text{-e}$ and PDV, but the correlation coefficient between AMV and PDV is -0.39 , suggesting that over the last century and half, AMV and PDV are in general negatively correlated to each other. Thus these two modes are not exactly orthogonal to each other. This could be interpreted as the potential interaction between these two modes or, as indicated by recent studies,^{21–23} these could be mode mixing. Either way, more research is needed to disentangle the relationship between AMV and PDV.

As shown in the 9 equations above, the contribution of $\text{CO}_2\text{-e}$ to the global mean, or northern/southern Hemisphere mean SAT, is the largest

among CO₂-e, AMV and PDV. From the changes of the regression coefficients, it suggests that the contribution of AMV to the SAT changes in the past century-and-a-half is larger than PDV's.

DATA AVAILABILITY

HADSST and HadsST3 data sets can be found at <https://www.metoffice.gov.uk/hadobs/hadcrut4/>. National Aeronautics and Space Administration (NASA) Goddard Institute for Space Studies (GISS) Surface Temperature Analysis dataset from 1881 to 2017 can be found at <https://data.giss.nasa.gov/gistemp/>. Coupled Model Inter-comparison Project phase 5 model data can be found at https://cmip.llnl.gov/cmip5/data_portal.html. The CO₂ data is from https://www.esrl.noaa.gov/gmd/ccgg/trends/global.html#global_data. Other greenhouse gas data is based on IPCC AR5 <https://www.ipcc.ch/assessment-report/ar5/>.

CODE AVAILABILITY

All data processing codes are available if a request is sent to the corresponding authors.

ACKNOWLEDGEMENTS

This work was supported by The National Key Research and Development Program of China (2016YFA0602100). Authors acknowledge the World Climate Research Programme's (WCRP) Working Group on Coupled Modelling (WGCM) for producing the CMIP5 model simulations and making them available for analysis. G.A.M. and A.H. are supported by the Regional and Global Model Analysis (RGMA) component of the Earth and Environmental System Modeling Program of the U.S. Department of Energy's Office of Biological and Environmental Research (BER) Cooperative Agreement #DE-FC02-97ER62402, and the National Science Foundation. The National Center for Atmospheric Research is sponsored by the National Science Foundation of the US.

AUTHOR CONTRIBUTIONS

T.W. initiated this work, F.G. and J.Z. did most of the data analysis, A.H. and G.A.M. helped to shape the ideas. All authors contributed actively to writing this work. T.W. and A.H. are both corresponding authors of this work.

ADDITIONAL INFORMATION

Supplementary Information accompanies the paper on the *npj Climate and Atmospheric Science* website (<https://doi.org/10.1038/s41612-019-0075-7>).

Competing interests: The authors declare no competing interests.

Publisher's note: Springer Nature remains neutral with regard to jurisdictional claims in published maps and institutional affiliations.

REFERENCES

- Lean, J. L. & Rind, D. H. How natural and anthropogenic influences alter global and regional surface temperatures: 1889 to 2006. *Geophys. Res. Lett.* **35**, L18701 (2008).
- Easterling, D. R. & Wehner, M. E. Is the climate warming or cooling? *Geophys. Res. Lett.* **36**, L08706 (2009).
- Santer, B. D., Mears, C., Doutriaux, C., Caldwell, P. & Gleckler et al. Separating signal and noise in atmospheric temperature changes: the importance of time-scale. *J. Geophys. Res.* **116**, D22105 (2011).
- Zhou, J. & Tung, K. K. Deducing the multi-decadal anthropogenic global warming trend using multiple regression analysis. *J. Atmos. Sci.* **70**, 3–8 (2013).
- Watanabe, M. et al. Contribution of natural decadal variability to global warming acceleration and hiatus. *Nat. Clim. Change* **4**, 893–897 (2014).
- Yan, X.-H. et al. The global warming hiatus: slowdown or redistribution? *Earth's Future* **4**, 1–11 (2016).
- Fyfe, J. C. et al. Making sense of the early-2000s warming slowdown. *Nat. Clim. Change* **6**, 224–228 (2016).
- Medhaug, I., Martin, B. S., Erich, M. F. & Knutti, R. Reconciling controversies about the 'global warming hiatus'. *Nature* **545**, 41–47 (2017).
- Hedemann, C., Mauritsen, T., Jungclaus, J. & Marotzke, J. The subtle origins of surface-warming hiatuses. *Nat. Clim. Change* **7**, 336–339 (2017).
- Rahmstorf, S., Foster, G. & Cahill, N. Global temperature evolution: recent trends and some pitfalls. *Environ. Res. Lett.* **12**, 054001 (2017).
- Zhang, Y., Wallace, J. M. & Battisti, D. S. ENSO-like interdecadal variability: 1900–93. *J. Clim.* **10**, 1004–1020 (1997).
- Power, S., Casey, T., Folland, C., Colman, A. & Mehta, V. Inter-decadal modulation of the impact of ENSO on Australia. *Clim. Dyn.* **15**, 319–324 (1999).
- Meehl, G. A., Arblaster, J. M., Fasullo, J. T., Hu, A. & Trenberth, K. E. Model-based evidence of deep-ocean heat uptake during surface-temperature hiatus periods. *Nat. Clim. Change* **1**, 360–364 (2011).
- Kosaka, Y. & Xie, S.-P. Recent global-warming hiatus tied to equatorial Pacific surface cooling. *Nature* **501**, 403–407 (2013).
- Fyfe, J. C. & Gillett, N. P. Recent observed and simulated warming. *Nat. Clim. Change* **4**, 150–151 (2014).
- Dong, B. & Dai, A. The influence of the interdecadal Pacific oscillation on temperature and precipitation over the globe. *Clim. Dyn.* **45**, 2667–2681 (2015).
- Meehl, G. A., Hu, A., Santer, B. D. & Xie, S.-P. Contribution of the interdecadal pacific oscillation to twentieth-century global surface temperature trends. *Nat. Clim. Change* **6**, 1005–1008 (2016).
- Knutson, T. R., Zhang, R. & Horowitz, L. W. Prospects for a prolonged slowdown in global warming in the early 21st century. *Nat. Comm.* **7**, 13676 (2016).
- Yao, S.-L., Luo, J.-J., Huang, G. & Wang, P. Distinct global warming rates tied to multiple ocean surface temperature changes. *Nat. Clim. Change* **7**, 486–491 (2017).
- Deser, C. & Blackmon, M. L. Surface climate variations over the North Atlantic Ocean during winter: 1900–1989. *J. Clim.* **6**, 1743–1753 (1993).
- Enfield, D. B., Mestas-Nunez, A. M. & Trimble, P. J. The atlantic multidecadal oscillation and its relationship to rainfall and river flows in the continental U.S. *Geophys. Res. Lett.* **28**, 2077–2080 (2001).
- Chylek, P., Klett, J. D., Lesins, G., Dubey, M. K. & Hengartner, N. The Atlantic multidecadal oscillation as a dominant factor of oceanic influence on climate. *Geophys. Res. Lett.* **41**, 1689–1697 (2014).
- Solomon, S. et al. Contributions of stratospheric water vapor to decadal changes in the rate of global warming. *Science* **327**, 1219–1223 (2010).
- Tung, K.-K. & Zhou, J. Using data to attribute episodes of warming and cooling in instrumental records. *PNAS* **110**, 2058–2063 (2013).
- DelSole, T., Tippett, M. K. & Shukla, J. A significant component of unforced multidecadal variability in the recent acceleration of global warming. *J. Clim.* **24**, 909–926 (2011).
- Chen, X. & Tung, K. K. Global mean surface temperature variability space-time perspective from rotated EOFs. *Clim. Dyn.* **51**, 1719–1732 (2018).
- Chen, X., Wallace, J. M. & Tung, K. K. Pair-wise rotated EOF of global SST anomaly. *J. Clim.* **30**, 5473–5489 (2017).
- Tung, K. K., Chen, X., Zhou, J. & Li, K.-F. Interdecadal variability in pan-Pacific and global SST, revisited. *Clim. Dyn.* **52**, 2145–2157 (2019).
- Kaufmann, R. K., Kauppi, H., Mann, M. L. & Stock, J. H. Reconciling anthropogenic climate change with observed temperature 1998–2008. *PNAS* **108**, 11790–11793 (2011).
- Solomon, S. et al. The persistently variable "background" stratospheric aerosol layer and global climate change. *Science* **333**, 866–870 (2011).
- Santer, B. D. et al. Volcanic contribution to decadal changes in tropospheric temperature. *Nat. Geosci.* **7**, 185–189 (2014).
- Kopp, G. & Lean, J. L. A new, lower value of total solar irradiance: evidence and climate significance. *Geophys. Res. Lett.* **38**, L01706 (2011).
- Fyfe, J. C., Salzen, K., von, Cole, J. N. S., Gillett, N. P. & Vernier, J.-P. Surface response to stratospheric aerosol changes in a coupled atmosphere–ocean model. *Geophys. Res. Lett.* **40**, 584–588 (2013).
- Trenberth, K. E. & Fasullo, J. T. An apparent hiatus in global warming? *Earth's Future* **1**, 19–32 (2013).
- Guemas, V., Doblas-Reyes, F. J., Andreu-Burillo, I. & Asif, M. Retrospective prediction of the global warming slowdown in the past decade. *Nat. Clim. Change* **3**, 649–653 (2013).
- Watanabe, M. et al. Strengthening of ocean heat uptake efficiency associated with the recent climate hiatus. *Geophys. Res. Lett.* **40**, 3175–3179 (2013).
- England, M. H. et al. Recent intensification of wind-driven circulation in the Pacific and the ongoing warming hiatus. *Nat. Clim. Change* **4**, 222–227 (2014).
- Chen, X. & Tung, K.-K. Varying planetary heat sink led to global-warming slowdown and acceleration. *Science* **345**, 897–903 (2014).
- Oka, A. & Watanabe, M. The post-2002 global surface warming slowdown caused by the subtropical Southern Ocean heating acceleration. *Geophys. Res. Lett.* **44**, 3319–3327 (2017).
- Drijfhout, S. The relation between natural variations in ocean heat uptake and global mean surface temperature anomalies in CMIP5. *Sci. Rep.* **8**, 7402, <https://doi.org/10.1038/s41598-018-25342-7> (2018).
- Dai, A., Fyfe, J. C., Xie, S.-P. & Dai, X. Decadal modulation of global-mean temperature by internal climate variability. *Nat. Clim. Change* **5**, 555–559 (2015).
- Meehl, G. A., Hu, A. & Teng, H. Initialized decadal prediction for transition to positive. *Nat. Comm.* **7**, 11718 (2016).

43. Schlesinger, M. E. An oscillation in the global climate system of period 65–70 years. *Nature* **367**, 723–726 (1994).

44. Swanson, K. L., Sugihara, G. & Tsonis, A. A. Long-term natural variability and 20th century climate change. *PNAS* **106**, 16120–16123 (2009).

45. Hunt, B. G. The role of natural climatic variation in perturbing the observed global mean temperature trend. *Clim. Dyn.* **36**, 509–521 (2011).

46. Loehle, C. Global temperature trends adjusted for unforced variability. *Univers. J. Geosci.* **3**, 183–187 (2015).

47. Wu, Z., Huang, N. E., Wallace, J. M., Smoliak, B. V. & Chen, X. On the time-varying trend in global-mean surface temperature. *Clim. Dyn.* **37**, 759–773 (2011).

48. Mann, M. E., Steinman, B. A. & Miller, S. K. Predictability of the recent slowdown and subsequent recovery of large-scale surface warming using statistical methods. *Geophys. Res. Lett.* **41**, 3211–3219 (2014).

49. Macias, D., Stips, A. & Garcia-Gorriz, E. Application of the singular spectrum analysis technique to study the recent hiatus on the global surface temperature record. *PLoS ONE* **9**, e107222 (2014).

50. Stips, A., Macias, D., Coughlan, C., Garcia-Gorriz, E. & Liang, X. S. On the causal structure between CO₂ and global temperature. *Sci. Rep.* **6**, 21691 (2016).

51. Lovejoy, S. Scaling fluctuation analysis and statistical hypothesis testing of anthropogenic warming. *Clim. Dyn.* **42**, 2339–2351 (2014).

52. Morice, C. P., Kennedy, J. J., Rayner, N. A. & Jones, P. D. Quantifying uncertainties in global and regional temperature change using an ensemble of observational estimates: The HadCRUT4 data set. *J. Geophys. Res.* **117**, D08101 (2012).

53. IPCC. Climate Change 2013: The Physical Science Basis. In *Contribution of Working Group I to the Fifth Assessment Report of the Intergovernmental Panel on Climate Change*. (eds Stocker, T. F. et al.) (Cambridge University Press, Cambridge, 2013).

54. Taylor, K. E., Stouffer, R. J. & Meehl, G. A. An overview of CMIP5 and the experiment design. *Bull. Am. Meteorol. Soc.* **93**, 485–498 (2012).

55. Gregory, J. M., Andrew, T., Good, P., Mauritzen, T. & Forster, P. M. Small global-mean cooling due to volcanic radiative forcing. *Clim. Dyn.* **47**, 3979–3991 (2016).

56. Trenberth, K. & Shea, D. J. Atlantic hurricanes and natural variability in 2005. *Geophys. Res. Lett.* **33**, L12704 (2005).

57. Meehl, G. A. & Hu, A. The mid-1970s climate shift in the pacific and the relative roles of forced versus inherent decadal variability. *J. Clim.* **22**, 780–792 (2009).

58. Comiso, J. C. et al. Positive trend in the Antarctic sea ice cover and associated changes in surface temperature. *J. Clim.* **30**, 2251–2267 (2017).

59. Hu, S. & Fedorov, A. V. The extreme El Niño of 2015–2016 and the end of global warming hiatus. *Geophys. Res. Lett.* **44**, 3816–3824 (2017).

60. Wang, C., Dong, S., Evan, A. T., Foltz, G. R. & Lee, S.-K. Multidecadal covariability of North Atlantic sea surface temperature, African dust, Sahel rainfall and Atlantic hurricanes. *J. Clim.* **25**, 5404–5415 (2012).

61. Knight, J. R., Allan, R. J., Folland, C. K., Vellinga, M. & Mann, M. E. A signature of persistent natural thermohaline circulation cycles in observed climate. *Geophys. Res. Lett.* **32**, L20708 (2005).

62. Maher, N., Gupta, A. S. & England, M. H. Drivers of decadal hiatus periods in the 20th and 21st centuries. *Geophys. Res. Lett.* **41**, 5978–5986 (2014).

63. Sun, C. et al. Western tropical Pacific multidecadal variability forced by the Atlantic multidecadal oscillation. *Nat. Commun.* **8**, 15998, <https://doi.org/10.1038/ncomms15998> (2017).

64. Sun, C., Li, J., Ding, R. Q. & Jin, Z. Cold season Africa–Asia multidecadal teleconnection pattern and its relation to the Atlantic multidecadal variability. *Clim. Dyn.* **48**, 3903–3918 (2017).

65. Sun, C. et al. Recent acceleration of Arabian Sea warming induced by the Atlantic–western Pacific trans-basin multidecadal variability. *Geophys. Res. Lett.* **46**, 1662–1671 (2019).

66. Sun, C. et al. Oceanic forcing of the interhemispheric SST dipole associated with the Atlantic Multidecadal Oscillation. *Environ. Res. Lett.* **13**, 074026 (2018).

67. Si, D. & Ding, Y. Oceanic forcings of the interdecadal variability in East Asian summer rainfall. *J. Clim.* **29**, 7633–7649 (2016).

68. Kerr, R. A. A North Atlantic climate pacemaker for the centuries. *Science* **288**, 1984–1986 (2000).

69. Deser, C., Alexander, M. A., Xie, S.-P. & Phillips, A. S. Sea surface temperature variability: patterns and mechanisms. *Annu. Rev. Mar. Sci.* **2**, 115–143 (2010).

70. Kennedy, J. J., Rayner, N. A., Smith, R. O., Saunby, M. & Parker, D. E. Reassessing biases and other uncertainties in sea-surface temperature observations since 1850 part 1: measurement and sampling errors. *J. Geophys. Res.* **116**, D14103 (2011).

71. Kennedy, J. J., Rayner, N. A., Smith, R. O., Saunby, M. & Parker, D. E. Reassessing biases and other uncertainties in sea-surface temperature observations since 1850 part 2: biases and homogenisation. *J. Geophys. Res.* **116**, D14104 (2011).

72. Hansen, J., Ruedy, R., Sato, M. & Lo, K. Global surface temperature change. *Rev. Geophys.* **48**, RG4004 (2010).

73. GISTEMP Team. GISS Surface Temperature Analysis (GISTEMP). NASA Goddard Institute for Space Studies. Dataset accessed 20YY-MM-DD. <https://data.giss.nasa.gov/gistemp/> (2018).

74. Rayner, N. A. et al. Global analyses of sea surface temperature, sea ice, and night marine air temperature since the late nineteenth century. *J. Geophys. Res.* **108**, 4407, <https://doi.org/10.1029/2002JD002670> (2003).

75. Meinshausen, M. et al. The R. C. P. greenhouse gas concentrations and their extension from 1765 to 2300. *Clim. Change* **109**, 213 (2011).

76. Henley, B. J. et al. A tripole index for the interdecadal pacific oscillation. *Clim. Dyn.* **45**, 3077–3090 (2015).

77. Booth, B. B., Dunstone, N. J., Halloran, P. R., Andrews, T. & Bellouin, N. Aerosols implicated as a prime driver of twentieth-century North Atlantic climate variability. *Nature* **484**, 228–232 (2012).



Open Access This article is licensed under a Creative Commons Attribution 4.0 International License, which permits use, sharing, adaptation, distribution and reproduction in any medium or format, as long as you give appropriate credit to the original author(s) and the source, provide a link to the Creative Commons license, and indicate if changes were made. The images or other third party material in this article are included in the article's Creative Commons license, unless indicated otherwise in a credit line to the material. If material is not included in the article's Creative Commons license and your intended use is not permitted by statutory regulation or exceeds the permitted use, you will need to obtain permission directly from the copyright holder. To view a copy of this license, visit <http://creativecommons.org/licenses/by/4.0/>.

© The Author(s) 2019